Jurnal Tribologi 40 (2024) 95-119

Jurnal Tribologi
Website : jurnaltribologi.mytribos.org
e-issn: 2289-7232

Multi-objective optimization of multi-stage Wind Turbine Gearbox (WTG) with macro-geometry and scuffing constraint

Ashish Kumar [1], Ramkumar Penchaliah [2*], Shankar Krishnapillai [1]

[1] Mechanical Design Optimization Lab, Machine Design Section, Department of Mechanical Engineering, Indian Institute of Technology Madras (IITM), INDIA.
[2] Advanced Tribology Research Lab (ATRL), Machine Design Section, Department of Mechanical Engineering, Indian Institute of Technology Madras (IITM), INDIA.
*Corresponding author: ramkumar@iitm.ac.in

KEYWORD

Planetary gear train
Helical gears
Multi-objective optimization
NSGA-II
Scuffing
Spur gears

ABSTRACT

This work executes a novel multi-objective optimization for a multi-stage Wind Turbine Gearbox (WTG), using a Non-Dominated Sorting Genetic Algorithm (NSGA-II) optimization technique with scuffing constraint for three different involute gear profiles: unmodified (U), smooth meshing (SM), and high load capacity (HLC). Further, ISO VG PAO synthetic-based oils are used for the WTG at a given rated speed. Two objective functions, namely, weight and power loss minimization are constructed with various traditional design constraints related to mechanical and scuffing wear. The result of one spur gear pair is validated with commercial gear software KISSsoft using ISO VG 460 mineral oil and obtained 0.605% efficiency improvement with scuffing constraint. Further, results with and without scuffing clearly shows that PAO 680 is the best-performing oil among the other oils. Based on the performance and Pareto front of the PAO 680, obtained minimum weight and power loss with scuffing is 7215.44 kg and 17.61 kW for high load capacity gear tooth profile.

Received 28 July 2023; received in revised form 3 November 2023; accepted 12 January 2024.
To cite this article: Kumar et al., (2024). Multi-objective optimization of multi-stage Wind Turbine Gearbox (WTG) with macro-geometry and scuffing constraint. Jurnal Tribologi 40, pp.95-119.

1.0 INTRODUCTION

In wind turbines, most failures are associated with the gearbox and cause 95% of downtime (Tavner, 2011). Due to tribological behavior and environmental changes, critical components such as gears, shafts, and bearings are affected. So, to improve life, gearbox design concerning scuffing wear needs to be focused on first. Today, many gearboxes are designed with regular mechanical design constraints only with an overall transmission ratio of more than 1:80, which can have more than 12 bearings and over 8 gear meshes. Hence, the WTG's significant challenges are minimizing the weight and power loss by including tribological constraints.

In an early study, (Li et al., 2012) optimized a 300-kW wind turbine gearbox with the objective of life design. MATLAB genetic algorithm toolbox was used for the set of design constraints such as gear ratio limit, pinion teeth, space limit, tooth width, and division helix angle for a given problem. Later, (Akay et al., 2013) minimized the volume of the gearbox by optimizing the gear ratio. Combined, two stages of a planetary gear train and one parallel stage of a helical gear pair model was set for the analysis. To investigate the load and load response, a dynamic multi-model gearbox was used. In terms of complication, (Tian & Tan, 2014) optimized the wind turbine gearbox using an improved genetic algorithm. Various mechanical design constraints such as contact ratio, meshing angle range, and several teeth constraints were applied for the combined two stages of planetary geartrain and 1 stage of helical gear pair. Finally, after improvement, it was found that the volume of the transmission system had been reduced significantly. However, constraints like interference, shaft constraints, and tribological constraints were not studied in detail. Choosing micro pitting as a design criterion, (Dinner, 2011) optimized the gear geometry.

The calculation approach had relied on the safety factor that must be greater than the required factor of safety. As per the latest scenario, (Ukonsaari & Bennstedt, 2016) presented a tool to calculate reliability by considering factors like oil cleanliness and viscosity for a typical and modern simplified gearbox. For this, a typical 2 MW power capacity wind turbine gearbox considering three stages (one stage of planetary and two stages of helical gear pair) was executed for the analysis. Different levels of road, as well as the absolute number of run hours, were inspected. Also, more concern was given to the gearbox's reliability and life in that study. However, the weight, space, efficiency, and transmission error of the gearbox were not analyzed in depth. (Fernandes et al., 2016) speculated the power loss for a 2.5MW wind turbine gearbox by comparing MIN, PAO, and PAG oil. Based on the tooth geometry modification, it was observed that efficiency improved by 0.8%. Recently, authors (Liu et al., 2021) considered the dynamic reliability constraints and reduced the volume of the gearbox by using Genetic Algorithm (GA). It was found that volume decreased by 3.58%. However, the detailed attributes of the tribological aspect were not included. With the trend, (Fotso et al., 2021)used ANN approach to predict load-dependent power loss .i.e., bearing power loss in wind turbines, and showed the effectiveness of the approach over actual bearing power loss. Lately, (Ziat et al., 2022) considered two objective functions, i.e., minimized the weight and maximized the efficiency. Only two stages of the planetary gear system were incorporated for gearbox design. Constraints such as dimensional, kinematic, etc., were used in the optimization part. But the study was limited to continuously variable transmission (CVT) problems which included various design variables such as face width, number of teeth for sun, planet, and ring gears, module, etc. were considered during optimization in the NSGA-II algorithm. Concerning complexity, the authors (Kumar et al., 2023) optimized the 3-stage WTG, and the results indicated that the design could fail if the tribological constraint was not incorporated. Along with this, many researchers worldwide optimized the simple and planetary gearbox as well. Literature showed that authors (Patil et al., 2019) optimized the

gearbox with NSGA-II, and it was found that there was a high risk of gearbox failure in terms of wear without consideration of scuffing and wear constraints. Further, (Parmar et al., 2020) used a discrete version of NSGA-II and optimized the planetary gearbox with a comprehensive list of constraints. In one of the studies, (Miler et al., 2017) minimized the gearbox volume and compared the results with commercial gear software KISSsoft. Also, (Kamble et al., 2022) did an experimental investigation on gearbox oil and observed that adding composite additives had less influence on the coefficient of friction and wear, which led to a reduction of 1.4% and 13.4%, respectively.

It could be inferred from the aforesaid literature that optimization of a complete multi-stage WTG (gears, shafts, and bearings together) by considering regular mechanical design constraints, critical planetary constraints, and scuffing constraint for the range of three PAO oils with two conflicting objective functions: power loss and weight was never reported, which is the originality of the present paper. Also, it is seen that based on mathematical benchmark tests on many algorithms, NSGA-II has outperformed the other algorithms. Further, it is more robust than others and has been reliably implemented for mixed variable types (discrete, integer, and continuous), which is essential for gear optimization. Hence, NSGA-II is preferred for the optimization. For validation, a single objective optimization for the spur gear pair problem has been carried out with all regular mechanical design and scuffing constraints, and results are validated with commercial gear software KISSsoft. For the design, almost all regular mechanical constraints are constructed as per AGMA standards (AGMA 6123-C16, 2016; AGMA 925-A03, 2001; American Gear Manufactures Association, 2004; Awea, 2010).

2.0 PROBLEM STATEMENT

The current paper aims to minimize WTG's weight and power loss by including various regular mechanical design constraints, critical planetary constraints, and scuffing constraint using the NSGA-II optimization algorithm. Detailed information of NSGA-II can be found in (Deb, 2011). Two planetary stages and one helical gear pair stage (pph) are used for the analysis for a 1.0 MW power capacity wind turbine to minimize the fitness function. The line diagram for the same is shown in Figure 1. Here, input will be given to the carrier, which transmits the power, and output will be taken from the third stage of helical gear, which is further linked with the generator through a high-speed shaft. Additionally, the subsequent stage will use the output from the previous stage as its input. A spherical roller bearing with the designation 22322E (to accompany heavy axial loads and shaft misalignment) is selected, as shown in Table 1 from the SKF bearing catalog (SKF, 2018). Detailed design parameters and various factors included in the simulations, like gear material, shaft material, safety factor, and power capacity, are given in Table 2 and other parameters are given in Appendix A.

Table 1: Spherical roller bearing dimension and load rating for WTG (SKF, 2018).

Bearing Designation	**C [kN]**	**d [mm]**	**D [mm]**	**D_1 [mm]**	**d_2 [mm]**	**B_b [mm]**	**M_b [kg]**
22322E	989	110	240	204	143.00	80	18.40

Table 2: Design parameters for WTG.

Parameter	Symbol	Value
Power Capacity (kW)	P	1000
Carrier input speed (rpm)	n_1	18
Overall gear transmission ratio	u_o	70
Pressure angle (°)	α	20
Material of gear	–	18CrNiMo7-6
Material of shaft	–	SAE 1095
Safety factor against bending	S_F	1.56
Safety factor against pitting	S_H	1.25
Safety factor for design of shaft	S_{FS}	2
Temperature of Oil [°C]	θ_{oil}	80
Number of planet gears in stage-I & stage-II	N_{CP}	3+3

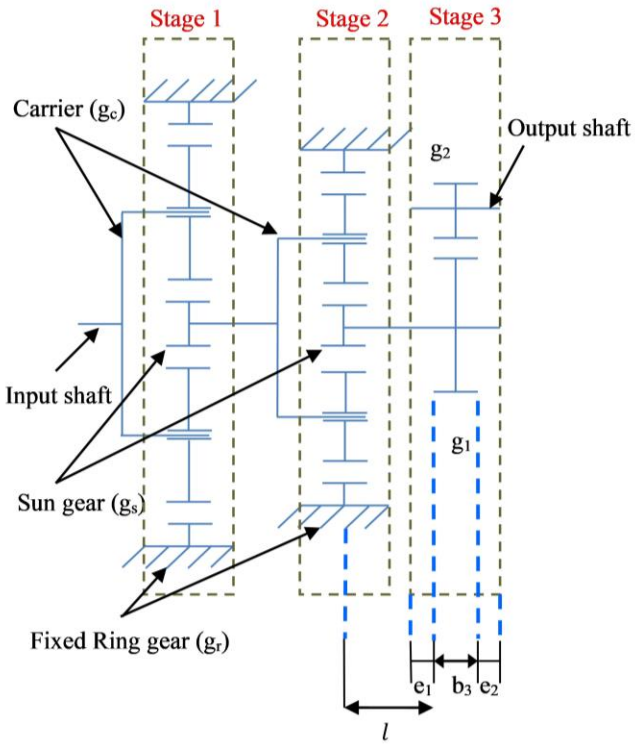

Figure 1: Line diagram for WTG arrangement.

3.0 OBJECTIVE FUNCTIONS

Two objective functions are constructed: a) Minimization of weight. b) Minimization of power loss.

3.1 Minimization of Weight

Weight reduction was the first goal function that was taken into account while mapping the three stages of the WTG. Weights of gears, shafts, and bearings are also included in the objective function. It does not consider the weight and design of the gearbox case for a wind turbine.

$$Min\ f_1(X) = W_{1^{st}stage} + W_{2^{nd}stage} + W_{3^{rd}stage} \tag{1}$$

$$W_{1^{st}/2^{nd}/3^{rd}stage} = W_{Gears} + W_{Shafts} + W_{Bearings} \tag{2}$$

where, weight of the gears, weight of the shafts and bearing are given Equations (3), (4), and (5).

$$W_{Gears} = \frac{\rho_{mg}\pi}{4}\begin{Bmatrix} b_1\left[\left(d_{s_1}^2 - d_{c2}^2\right) + N_{CP}\left(d_{p_1}^2 - D^2\right) + \left(d_{ro_1}^2 - d_{ri_1}^2\right)\right] \\ +b_2\left[\left(d_{s_2}^2 - d_{ss_2}^2\right) + N_{CP}\left(d_{p_2}^2 - D^2\right) + \left(d_{ro_2}^2 - d_{ri_2}^2\right)\right] \\ +b_3\left[\left(d_1^2 - d_{ss_2}^2\right) + \left(d_2^2 - d_{ss_3}^2\right)\right] \end{Bmatrix} \tag{3}$$

$$W_{Shafts} = \frac{\rho_{ms}\pi}{4}\left[N_{CP}d^2(l_{p_1} + l_{p_2}) + L_2 d_{ss_2}^2 + L_3 d_{ss_3}^2\right] \tag{4}$$

$$W_{Bearings} = N_b M_b \tag{5}$$

where,

$$L_2 = l + b_3 + e_2 \tag{6}$$

$$L_3 = e_1 + b_3 + e_2 \tag{7}$$

e_1, e_2 represents respectively the space between the walls and gears and are kept as 10mm.

3.2 Minimization of Power Loss

The second competing objective function for the investigation is the reduction of power loss. This analysis for multi-stage WTG considers losses for all three stages that are both load-dependent (bearing friction loss and gear mesh friction loss) and non-load-dependent (contact oil seal) losses. Churning and pocketing losses, which are insignificant compared to other power losses, are not considered.

$$Min\ f_2(X) = P_{I^{st}stage} + P_{2^{nd}stage} + P_{3^{rd}stage} \tag{8}$$

$$P_{1^{st}/2^{nd}/3^{rd}stage} = P_{VZP} + P_{VL} + P_{VD} \tag{9}$$

Gear mesh friction loss can be calculated from the ohlendorf equation(Fernandes et al., 2015) as shown in Equation (10).

$$P_{VZP} = P\mu_{mz}H_V \tag{10}$$

Where, P, μ_{mz} are input power and coefficient of friction and can be calculated as per Schlenck's approach which is given in Equation (11),

$$\mu_{mz} = 0.048\left(\frac{\left(\frac{F_{bt}}{b}\right)}{v\sum c\rho_{red}c}\right)^{0.2} \eta^{0.05}R_a^{0.25}X_L \tag{11}$$

Where, $\frac{F_{bt}}{b}, R_a, \eta, \rho_{redC}$ are the force per unit width, surface roughness, oil viscosity used and radius of curvature respectively. The value of X_L for PAO oil is drawn from the experimental results (Fernandes et al., 2015) and depends on the kind of lubricant utilized during the investigation. H_V stands for the gear loss factor, which is calculated using Equation (12),

$$H_V^{Ohlendorf} = \frac{(1+u)\pi}{Z_1\, cos(\beta_{zb})}(1 - \epsilon_\alpha + \epsilon_1^2 + \epsilon_2^2) \tag{12}$$

where, $u, Z_1, \beta_{zb}, \epsilon_\alpha, \epsilon_1, \epsilon_2$ represents gear ratio, number of teeth on pinion, gear base helix angle, transverse contact ratio, addendum contact ratio of pinion and wheel respectively.

Bearing friction losses is calculated as per (Jelaska, 2012), which is shown in Equation (13),

$$P_{VL} = \mu F v \tag{13}$$

where, μ, F, v are friction coefficient, bearing load and velocity. For this study, spherical roller bearing with $\mu = 0.0021$ is used.

The Simrit equation calculates contact oil seal loss (Fernandes et al., 2016). The seal loss is represented by Equation (14), and it solely depends on the shaft diameter d_{ss} and rotational speed n.

$$P_{VD} = 7.69 \times 10^{-6} d_{ss}^2 n \tag{14}$$

3.3 Constraint Formulation

All regular mechanical design constraints, critical planetary gears constraints, and the scuffing constraint are discussed in this section.

Bending strength as per (American Gear Manufactures Association, 2004)is given by Equation (15),

$$F_t K_o K_v K_s \frac{1}{bm_t}\frac{K_H K_B}{Y_J} - \frac{\sigma_{FP} Y_N}{S_F Y_\theta Y_Z} \leq 0 \tag{15}$$

Pitting strength as per (American Gear Manufactures Association, 2004) is given by Equation (16),

$$Z_E\sqrt{F_t K_o K_v K_s\left(\frac{K_H Z_R}{d_w b\, Z_I}\right)} - \frac{\sigma_{HP} Z_N Z_W}{S_H Y_\theta Y_z} \leq 0 \tag{16}$$

where, d_w is operating pitch diameter and Z_E is elastic coefficient.
For helical gears,
d_w is operating pitch diameter of pinion.

For both stage 1 and stage 2 sun-planet mesh,

$$d_w = \frac{2a_e}{u_e + 1} \tag{17}$$

$$Z_E = \sqrt{\frac{1}{\pi\left(\frac{1-v_s^2}{E_s} + \frac{1-v_p^2}{E_p}\right)}} \tag{18}$$

For both stage 1 and stage 2 planet-ring mesh,

$$d_w = \frac{2a_i}{u_i - 1} \tag{19}$$

$$Z_E = \sqrt{\frac{1}{\pi\left(\frac{1-v_p^2}{E_p} + \frac{1-v_r^2}{E_r}\right)}} \tag{20}$$

Equation (21) and is used to prevent interference between the meshing gear teeth to obtain the minimum possible pinion teeth.

$$\frac{2}{(1+2u)\,sin^2\,\alpha_t}(u + \sqrt{(u^2 + (1+2u)\,sin^2\,\alpha_t)} - Z_{p\,or\,s} \leq 0 \tag{21}$$

Where, u is a stage gear ratio and $Z_{p\,or\,s}$ is the number of teeth for pinion, and sun gear.

Shaft diameter constraint is given by Equation (22),

$$\left[\frac{32S_{FS}}{\pi}\sqrt{\left(\frac{T}{S_y}\right)^2 + \left(\frac{M_{Max}}{S_e}\right)^2}\right]^{\frac{1}{3}} - d_{ss_i} \leq 0 \tag{22}$$

While determining the maximum bending moments for stage 3, the influence of the axial load that happened during helical gear meshing has also been considered.

Contact ratio constraint (Parmar et al., 2020) is given by Equation (23),

$$1.2 \leq C_{\alpha e}, C_{\alpha i}, C_{\alpha h} \leq 2 \tag{23}$$

For stage 1 and stage 2,

$$C_{\alpha e} = \frac{1}{P_b}\left[\frac{\sqrt{(d_{so}^2 - d_{sb}^2)}}{2} + \frac{\sqrt{d_{po}^2 - d_{pb}^2}}{2} - a_e\,sin\,\alpha_{wt}\right] \tag{24}$$

$$C_{\alpha i} = \frac{1}{P_b}\left[\frac{\sqrt{d_{po}^2 - d_{pb}^2}}{2} - \frac{\sqrt{d_{r0}^2 - d_{rb}^2}}{2} + a_i \sin \alpha_{wt}\right] \quad (25)$$

Where, P_b is determined from Equation (26),

$$P_b = \pi m \cos \alpha \quad (26)$$

For stage 3, the total contact ratio (AGMA 925-A03, 2001) for the helical gear pair is the sum of the transverse and axial contact ratios by Equation (27).

$$C_{\alpha h} = \varepsilon_\alpha + \varepsilon_\beta \quad (27)$$

$$\varepsilon_\alpha = \frac{1}{P_{bh}}\left[\frac{\sqrt{(d_{og}^2 - d_{bg}^2}}{2} + \frac{\sqrt{d_{op}^2 - d_{bp}^2}}{2} - a_1 \sin \alpha_t\right] \quad (28)$$

$$\varepsilon_\beta = \frac{b}{p_X} \quad (29)$$

Where, $\epsilon_\alpha, \epsilon_\beta, p_X$, are transverse contact ratio, axial contact ratio, and axial pitch. Where P_{bh} is calculated from the Equation (30).

$$P_{bh} = \pi m_t \cos \alpha \quad (30)$$

Face width constraint is given by Equation (31),

$$3\pi m \leq b \leq 5\pi m \quad (31)$$

Gear ratio constraint is given by Equation (32),

$$3 \leq u_1, u_2, u_3 \leq 6 \quad (32)$$

Equation (33) is used to avoid the hunting for minimum vibration,

$$Z_{i+1} \neq multiple\ (Z_i) \quad (33)$$

Maximum number of gear teeth is limited to 125, and constraint (Patil et al., 2019) is given by given by Equation (34),

$$Z_g - Z_{gmax} \leq 0 \quad (34)$$

For WTG, the overall gear transmission ratio constraint is set between ±5% clearance value (Li et al., 2012) as shown in Equation (35),

$$66.5 \leq u_o \leq 73.5 \quad (35)$$

For WTG, Equations (36), (37), (38) and (39) shows the geometric constraints,

For stage 1 and stage 2, width of the gears must be larger than the planet bearing width, as given in Equation (35). Also, root diameters of gears are kept greater than the shaft diameter used as shown in Equations (36) and (37),

$$b > B_b \tag{36}$$

$$d_{ss_i} \leq d_{rs} \tag{37}$$

$$d \leq d_{rp} \tag{38}$$

The face width for the first stage is kept greater to withstand high torques and moments as per (Kumar et al., 2023) shown in Equation (38),

$$b_1 > b_2 + b_3 \tag{39}$$

Equally spaced planet constraint is set as per (AGMA 6123-C16, 2016; Parmar et al., 2020) is shown in Equation (40),

$$\frac{Z_r + Z_s}{N_{CP}} = an\ integer \tag{40}$$

Non-factorizing state (AGMA 6123-C16, 2016; Parmar et al., 2020) is given by Equations (41),(42).

$$\frac{Z_r}{N_{CP}} \neq an\ integer \tag{41}$$

Or,

$$\frac{Z_s}{N_{CP}} \neq an\ integer \tag{42}$$

Coaxiality constraint (Parmar et al., 2020) is given by Equation (43),

$$d_s + 2d_p = d_r \tag{43}$$

3.3.1 Scuffing constraint

Scuffing is localized damage caused by solid-phase welding between surfaces in relative motion. Generally, scuffing occurs due to the breakdown of thin lubricant film under the starve or severe boundary lubrication regime. Further, it is accompanied by metal transfer from one surface to another due to intense frictional heat generated by a combination of high sliding velocity and high contact stress, ultimately leading to catastrophic failure.

The normal distribution of scuffing temperature is used to calculate the likelihood of scuffing failure for WTG separately for each step (Patil et al., 2019).

$$P_{scuf(e_1,e_2)}, P_{scuf(i_1,i_2)}, P_{scuf(h)} \leq 0.1 \tag{44}$$

The tooth's surface temperature θ_M just before it penetrates into the contact zone and the highest flash temperature $\theta_{fl\,max}$ along the line of action combine to form the maximum contact temperature. The maximum contact temperature is determined by Equation (45),

$$\theta_{B\,max} = \theta_M + \theta_{fl\,max} \tag{45}$$

Where Equation (46) determines the tooth surface temperature θ_M,

$$\theta_M = k_{sump}\theta_{oil} + 0.56\theta_{fl\,max} \tag{46}$$

The maximum flash temperature $\theta_{fl\,max}$ is computed from Blok's equation as per (AGMA 925-A03, 2001) shown in Equation (47),

$$\theta_{fl(i)} = 31.62K\mu_{m(i)}\frac{X_{\Gamma(i)}w_n}{\left(b_{H(i)}\right)^{0.5}}\frac{|v_{r1(i)} - v_{r2(i)}|}{B_{M1}\left(v_{r1(i)}\right)^{0.5} + B_{M2}\left(v_{r2(i)}\right)^{0.5}} \tag{47}$$

The scuffing temperature depends on the lubricant viscosity, as shown in Equation (48),

$$\theta_S = 118 + 33ln\,(v_{40}) \tag{48}$$

As a result, the scuffing can be expressed as a function of the design variables provided by Equations (49), (50) and (51), respectively.

$$P_{scuf(e)} = f\left(Z_s, Z_p, m, b, v\right) \tag{49}$$
$$P_{scuf(i)} = f(Z_p, Z_r, m, b, v) \tag{50}$$
$$P_{scuf\,(h)} = f(d, b, z, \eta, \beta) \tag{51}$$

4.0 DESIGN VARIABLES

For this WTG optimization problem, all 18 most influencing design variables are taken into consideration as per (Fernandes et al., 2016; Liu et al., 2021; Patil et al., 2019), which include module (m_1, m_2, m_3), the number of teeth for sun $(Z_{s_1}, \mathrm{Z_{s_2}})$, planet $(Z_{p_1}, \mathrm{Z_{p_2}})$, and ring gear $(Z_{r_1}, \mathrm{Z_{r_2}})$, the number of teeth for gear and pinion (Z_1, Z_2), face width for all the three stages (b_1, b_2, b_3), the diameter of shafts $(d_{ss2}, \mathrm{d_{ss_3}})$, helix angles (β_3) and helix direction (h_3). The detailed information is shown in Table 3. The design vector for the three stages of WTG is as follows,

$$X = \{m_1, m_2, m_3, Z_{s_1}, Z_{s_2}, Z_{p_1}, Z_{p_2}, Z_{r_1}, Z_{r_2}, Z_1, Z_2, b_1, b_2, b_3, d_{ss_2}, d_{ss_3}, \beta_3, h_3\}$$

Where a is,

$$a = \{1.125, 1.375, 1.75, 2.25, 2.75, 3.5, 4.5, 5.5, 6.5, 7, 9, 11, 14, 18, 22, 28\}$$

Table 3: Details of wind turbine gearbox design variables.

Design variable	Lower limit	Upper limit	Type
m_1, m_2, m_3	a^*	–	Discrete
Z_{s_1}, Z_{s_2}	15	70	Integer
Z_{p_1}, Z_{p_2}	30	80	Integer
Z_{r_1}, Z_{r_2}	80	200	Integer
Z_1	50	125	Integer
Z_2	18	70	Integer
b_1, b_2, b_3	30	600	Continuous
d_{ss_2}, d_{ss_3}	10	200	Integer
β_3	8	30	Continuous
h_3	1=Right hand helix	2=Left hand helix	

5.0 GEAR TOOTH PROFILE

The load-sharing factor must be determined to compute the flash temperature of a gear tooth, which is necessary to resolve the likelihood of scuffing or wear failure. Further, all the three profiles listed in (AGMA 925-A03, 2001) are used in this study. Figure 2 (a) shows the distances along the meshing gears' contact lines.

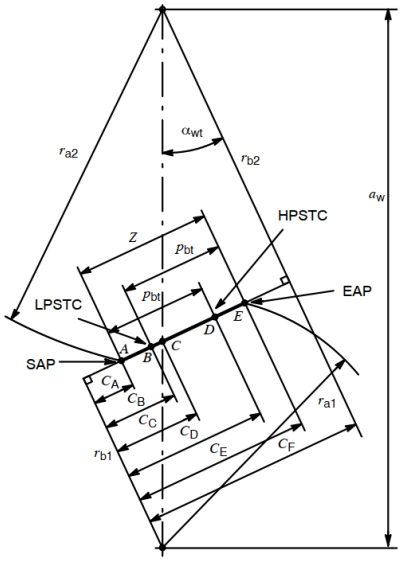

(a)

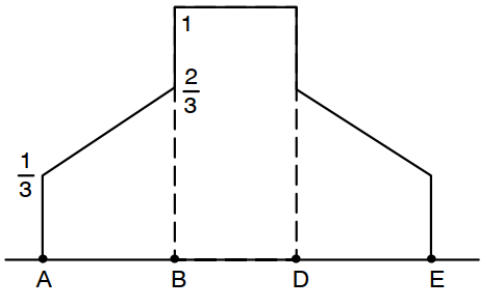

(b)

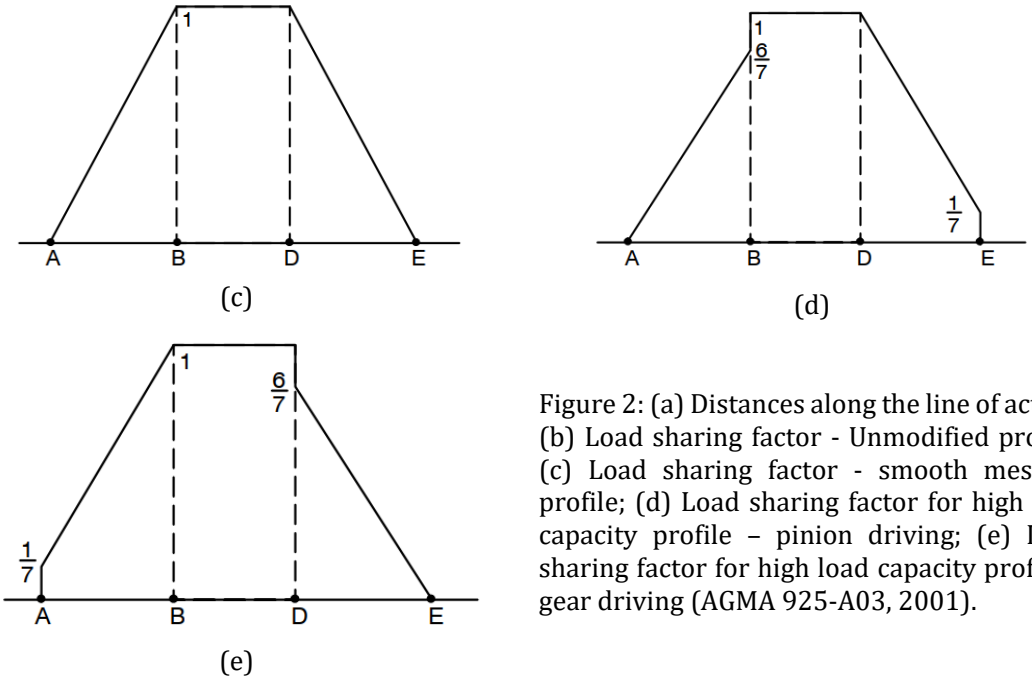

Figure 2: (a) Distances along the line of action; (b) Load sharing factor - Unmodified profile; (c) Load sharing factor - smooth meshing profile; (d) Load sharing factor for high load capacity profile – pinion driving; (e) Load sharing factor for high load capacity profile – gear driving (AGMA 925-A03, 2001).

5.1 Unmodified Gear Tooth Profile

If there is no relief at base or tip as shown in Figure 2(b). Load sharing factor for unmodified gear tooth profile is given by Equations (52), (53), and (54),

$$X_{\Gamma(i)} = \frac{1}{3} + \frac{1}{3}\left(\frac{\xi_i - \xi_A}{\xi_B - \xi_A}\right) \qquad for\ \xi_A \le \xi_i < \xi_B \tag{52}$$

$$X_{\Gamma(i)} = 1 \qquad for\ \xi_B \le \xi_i \le \xi_D \tag{53}$$

$$X_{\Gamma(i)} = \frac{1}{3} + \frac{1}{3}\left(\frac{\xi_E - \xi_i}{\xi_E - \xi_D}\right) \qquad for\ \xi_D < \xi_i \le \xi_E \tag{54}$$

5.2 Smooth Meshing Gear Tooth Profile

If adequate tip and root relief is designed for smooth meshing as shown in Figure 2(c). Load sharing factor for smooth meshing gear tooth profile is given by Equations (55), (56), and (57),

$$X_{\Gamma(i)} = \frac{\xi_i - \xi_A}{\xi_B - \xi_A} \qquad for\ \xi_A \le \xi_i < \xi_B \tag{55}$$

$$X_{\Gamma(i)} = 1 \qquad for\ \xi_B \le \xi_i \le \xi_D \tag{56}$$

$$X_{\Gamma(i)} = \frac{\xi_E - \xi_i}{\xi_E - \xi_D} \qquad for\ \xi_D < \xi_i \le \xi_E \tag{57}$$

5.3 High Load Capacity Gear Tooth Profile

If adequate tip and root relief is designed for high load capacity, and if the pinion drives the gear as shown in Figure 2(d). Load sharing factor is given by Equations (58), (59) and (60),

$$X_{\Gamma(i)} = \frac{6}{7}\left(\frac{\xi_i - \xi_A}{\xi_B - \xi_A}\right) \qquad for\ \xi_A \le \xi_i < \xi_B \tag{58}$$

$$X_{\Gamma(i)} = 1 \qquad for\ \xi_B \le \xi_i \le \xi_D \tag{59}$$

$$X_{\Gamma(i)} = \frac{1}{7} + \frac{6}{7}\left(\frac{\xi_E - \xi_i}{\xi_E - \xi_D}\right) \qquad for\ \xi_D < \xi_i \le \xi_E \tag{60}$$

If adequate tip and root relief is designed for high load capacity, and if the pinion is driven by the gear as shown in Figure 2(e). Similarly, load sharing factor here is given by Equations (61), (62), and (63),

$$X_{\Gamma(i)} = \frac{1}{7} + \frac{6}{7}\left(\frac{\xi_i - \xi_A}{\xi_B - \xi_A}\right) \qquad for\ \xi_A \le \xi_i < \xi_B \tag{61}$$

$$X_{\Gamma(i)} = 1 \qquad for\ \xi_B \le \xi_i \le \xi_D \tag{62}$$

$$X_{\Gamma(i)} = \frac{6}{7}\left(\frac{\xi_E - \xi_i}{\xi_E - \xi_D}\right) \qquad for\ \xi_D < \xi_i \le \xi_E \tag{60}$$

6.0 RESULTS AND DISCUSSION

Two cases are discussed here; Case (a): Results of single-objective optimization with weight as a primary criterion of one spur gear pair is validated with commercial gear software KISSsoft and Case (b): Multi-objective optimization results are compared for three different ISO VG PAO oils with and without scuffing constraint to find the best oil.

6.1 Case (a): Results of single-objective optimization with weight as a primary criterion of one spur gear pair is validated with commercial gear software KISSsoft

In this case, solutions obtained from commercial gear software KISSsoft, which supports rough sizing (raw gear dimensions) and fine sizing (macro gear geometry), are validated with numerical simulation of a single-objective optimization problem with weight as the essential criteria. One spur gear pair is simulated using ISO VG 460 mineral oil with an input power of 30kW at an input speed of 1000 rpm while considering all standard mechanical design constraints as well as scuffing constraints.

Table 4 demonstrates that module values obtained for unmodified, smooth meshing, and high-load capacity gear tooth profiles are the same when comparing the design with and without scuffing constraint. In addition, the set of minimal weight values has been chosen for validation through KISSsoft, and a single-objective problem's design variables are used to calculate the power loss by back substitution. Following substitution, it is noted that additional efficiency improvements of 0.605% for spur gear pair are attainable for all unmodified, smooth-mesh, high-load capacity gear profiles with all constraints, including scuffing. For brevity, only module and face with value of design variables are shown. Additionally, the design without scuffing constraint also yields a 0.605% increase in efficiency compared to KISSsoft, which may result from the optimization process skipping the scuffing restriction. Also, the risk of scuffing is calculated for

both designs, which shows that the design is safe and within the permissible limit with low scuffing risk, as shown in Table 4. Further, this problem is extended to more advanced gearboxes, like wind turbine gearboxes, which may have more than two stages. By considering two competing objective functions, analysis has been completed with the consideration of all constraints.

Table 4: Results validation with KISSsoft.

Single objective optimization of spur gear pair with scuffing constraint						
Profile	$\boldsymbol{m}(\boldsymbol{mm})$	$\boldsymbol{b}\ (\boldsymbol{mm})$	$\boldsymbol{w}\ (\boldsymbol{kg})$	$\boldsymbol{P_{loss}}\ (\boldsymbol{watt})$	$\boldsymbol{\eta}$ (%)	$\boldsymbol{P_{scuff\ (h)}}$(%)
Unmodified	2.75	31.36	8.25	86.18	99.70	05.00
Smooth meshing	2.75	31.26	8.23	86.23	99.70	05.00
High load capacity	2.75	31.34	8.24	86.19	99.70	05.00
Single objective optimization of spur gear pair without scuffing constraint						
–	2.75	31.23	8.22	86.25	99.70	05.00
KISSsoft						
–	2.50	29.79	8.07	–	99.10	05.00

6.2 Case (b)

6.2.1 Subcase 1: with scuffing constraint

In this subcase, the multi-objective problem of WTG is carried out for three gear tooth profiles: unmodified, smooth meshing, and high load capacity, with scuffing constraint. To determine the best synthetic gear oil, Pareto fronts from ISO VG PAO 220, 460, and 680 are compared. The Pareto front curve contains the optimal solution, which provides a set of non-dominated solutions from which the designer can choose depending on the situation. For the total weight and power loss for all the stages, the extreme left and right of the Pareto front provide a minimal fitness function value of WTG, respectively. If both solutions are equally compelling, the solution closest to the Utopia point, which provides a moderate value of both objective functions, should be preferred.

Figures 3, 4(a), and 4(b) shows Pareto fronts of various cases with scuffing constraints and different oils, showing weight and power loss. These Pareto curves ' extreme points differ depending on how much the criteria for other profiles are satisfied. Based upon these curves, Table 5 is obtained, which shows the minimum objective function values for weight and power loss with scuffing constraint. Furthermore, it can be seen that the performance of PAO 680, among other oils, is better for all three gear tooth profiles, implying minimum weight.

To withstand high torques, forces, and moments, large values of design variables such as module and face width are seen in stage 1 and stage 2, as given in Table 6 and Table 7. Also, Table 8 indicates low design variables result in high scuffing risk. Hence, net weight and power loss are attained based on these design variables, as shown in Table 5.

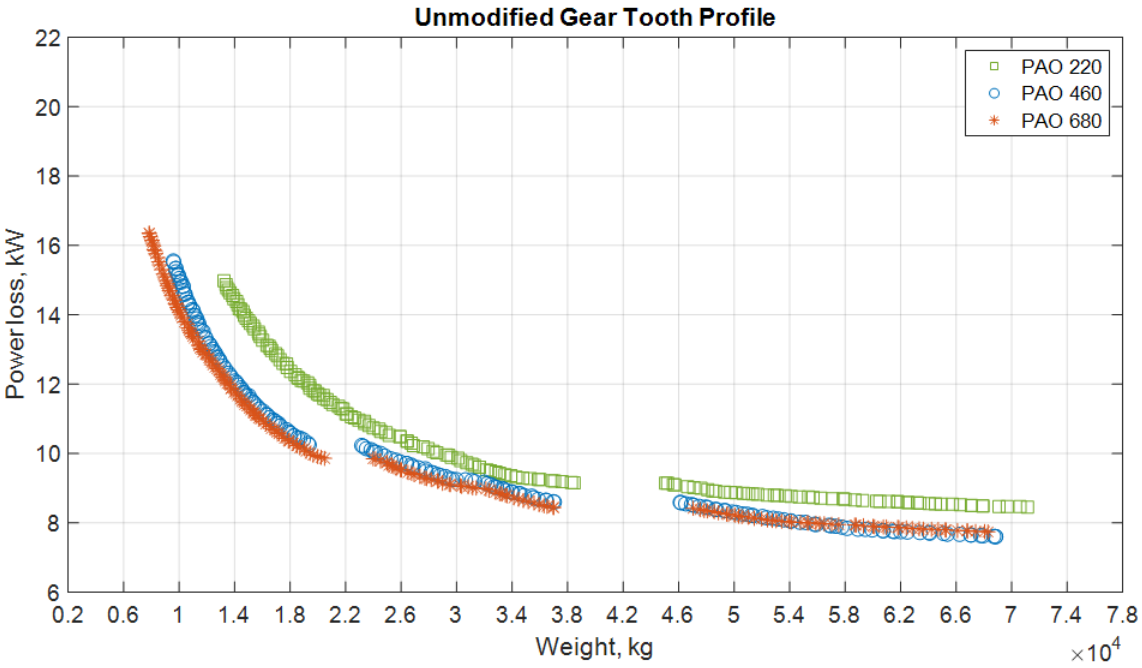

Figure 3: Pareto fronts for three different grades of oil for unmodified gear tooth profile.

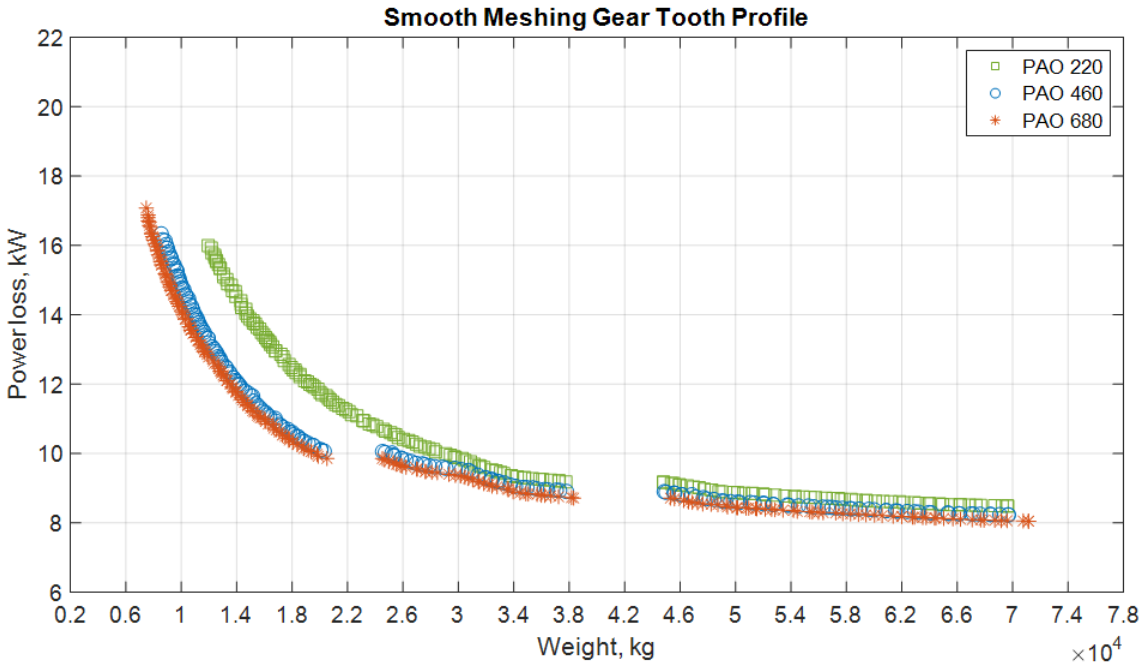

(a)

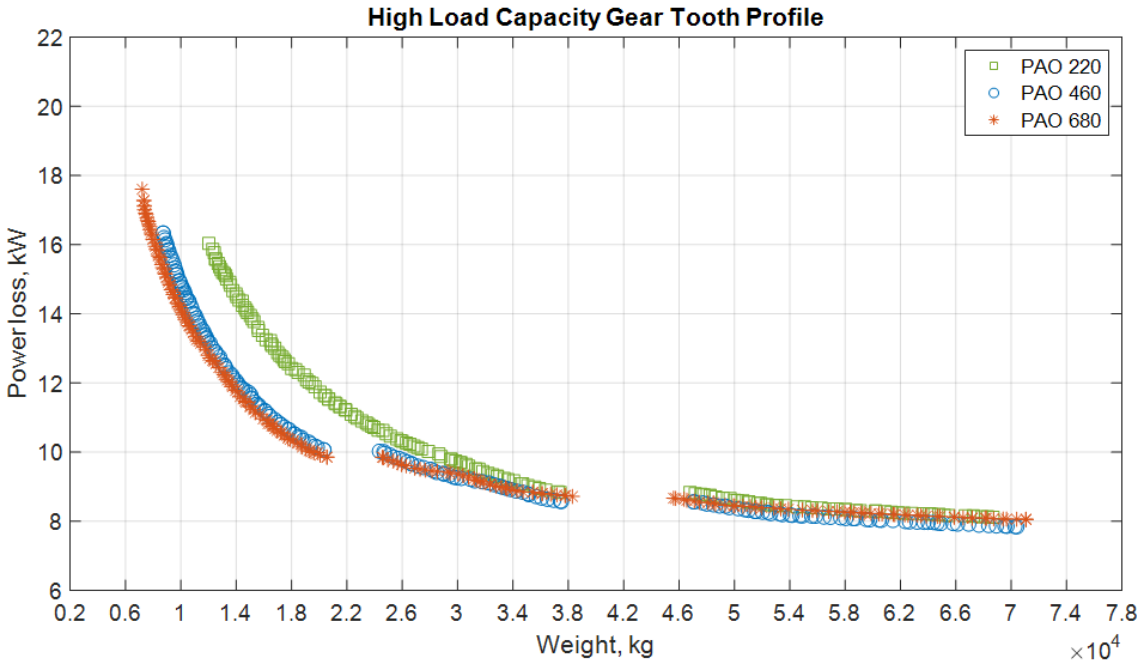

(b)

Figure 4: (a). Pareto fronts for three different grades of oil for smooth meshing gear tooth profile; (b). Pareto fronts for three different grades of oil for high load capacity gear tooth profile.

Table 5: Minimum objective function values for weight and power loss attained with scuffing constraint.

Profile	**Weight, kg**	**Power loss, kW**
PAO 220		
Unmodified	12988.90	15.13
Smooth meshing	11944.60	15.99
High load capacity	11889.50	16.15
PAO 460		
Unmodified	9579.41	15.55
Smooth meshing	8784.99	16.21
High load capacity	8556.12	16.34
PAO 680		
Unmodified	7842.28	16.35
Smooth meshing	7475.00	17.08
High load capacity	7215.44	17.61

Table 6: Design variables obtained for three gear tooth profiles with scuffing constraint for stage 1.

ISO VG	m_1	b_1	Z_{s_1}	Z_{p_1}	Z_{r_1}
Unmodified Gear Tooth Profile					
PAO 220	22	307.99	28	38	104
PAO 460	22	300.92	26	40	106
PAO 680	18	276.94	35	46	127
Smooth Meshing Gear Tooth Profile					
PAO 220	22	304.46	28	41	110
PAO 460	18	276.78	35	46	127
PAO 680	18	249.01	35	46	127
High Load Capacity Gear Tooth Profile					
PAO 220	22	310.59	28	38	104
PAO 460	18	278.48	34	47	128
PAO 680	18	275.12	35	46	127

Table 7: Design variables obtained for three gear tooth profiles with scuffing constraint for stage 2.

ISO VG	m_2	b_2	Z_{s_2}	Z_{p_2}	Z_{r_2}	d_{ss_2}
Unmodified Gear Tooth Profile						
PAO 220	18	201.38	40	47	134	69
PAO 460	14	194.02	40	41	122	55
PAO 680	14	187.38	40	53	146	39
Smooth Meshing Gear Tooth Profile						
PAO 220	18	196.46	41	43	127	39
PAO 460	18	188.29	40	44	128	37
PAO 680	14	170.23	40	44	128	24
High Load Capacity Gear Tooth Profile						
PAO 220	18	203.54	40	50	140	38
PAO 460	18	187.26	40	44	128	28
PAO 680	14	171.22	38	46	130	22

6.2.2 Subcase 2: without scuffing constraint

It describes the multi-objective optimization results without scuffing constraint for three different oil grades. Table 9 shows the risk of scuffing in WTG for all three stages determined by substituting the design variables attained in the absence of scuffing constraint.

In stage 1, it is observed that the probabilities of scuffing failure are within the permitted value for all three oils. Further, stage 2 results show that the risk of scuffing for PAO 220 is 8.23%, 8.23%, and 8.31% for sun-planet gear mesh. However, for planet-ring gear mesh it is 5% for unmodified, smooth meshing and high load capacity gear profile, which ultimately implies low scuffing risk. For stage 3, the risk probability is high, i.e., exceeds the permitted value. It might be due to the attainment of low design variables, high sliding velocities and high contact stress. At higher speeds, high friction heat gives rise to an increase in temperature, which later unable to separate contact surfaces. Separation of surfaces is based on the thickness of the lubricant, which is not sufficient at higher speeds, implying high scuffing risk as shown in Table 9. Further, it is noted

that risk of scuffing for PAO 220 and PAO 460 varies from moderate to high. However, risk for PAO 680 is close to the limited value of low scuffing risk due to the viscous nature.

Minimum objective function values for weight and power loss, without scuffing constraint for all three grade of oils is shown in Table 13, and Figure 5 show the Pareto fronts for all the oils. It is observed that PAO 680 outperforms the other lubricants and hence saves power loss as shown in Table 13. Tables 10, 11, and 12 show the design variables obtained after optimization with respect to all the three stages without scuffing constraint.

Table 8: Design variables obtained for three gear tooth profiles with scuffing constraint for stage 3.

ISO VG	m_3	b_3	Z_1	Z_2	β_3	h_3	d_{ss_3}
Unmodified Gear Tooth Profile							
PAO 220	11	106.12	101	31	8.000	2	15
PAO 460	11	105.45	102	32	8.002	1	10
PAO 680	9	087.33	102	33	8.000	1	12
Smooth Meshing Gear Tooth Profile							
PAO 220	11	107.79	105	31	8.009	2	12
PAO 460	9	087.12	106	31	8.004	2	14
PAO 680	7	069.44	103	30	8.000	2	13
High Load Capacity Gear Tooth Profile							
PAO 220	9	105.93	105	28	8.000	2	10
PAO 460	9	106.67	105	29	8.000	2	14
PAO 680	9	086.62	100	29	8.000	1	10

Table 9: Result of scuffing risk without considering scuffing constraint.

Profile	**Stage-I**		**Stage-II**		**Stage-III**
	$P_{scuff\,(e_1)}$ (%)	$P_{scuff\,(i_1)}$ (%)	$P_{scuff\,(e_2)}$ (%)	$P_{scuff(i_2)}$(%)	$P_{scuff\,(h3)}$(%)
PAO 220					
U	05.00	05.00	08.23	05.00	18.89
SM	05.00	05.00	08.23	05.00	65.07
HLC	05.00	05.00	08.31	05.00	67.61
PAO 460					
U	05.00	05.00	05.00	05.00	06.64
SM	05.00	05.00	05.00	05.00	31.38
HLC	05.00	05.00	05.00	05.00	33.31
PAO 680					
U	05.00	05.00	05.00	05.00	05.00
SM	05.00	05.00	05.00	05.00	09.56
HLC	05.00	05.00	05.00	05.00	10.92

Table 10: Design variables obtained without scuffing constraint for stage 1.

ISO VG	m_1	b_1	Z_{s_1}	Z_{p_1}	Z_{r_1}
PAO 220	14	188.89	47	58	163
PAO 460	14	179.66	49	59	167
PAO 680	14	202.06	47	55	157

Table 11: Design variables obtained without scuffing constraint for stage 2.

ISO VG	m_2	b_2	Z_{s_2}	Z_{p_2}	Z_{r_2}	d_{s2}
PAO 220	9	111.54	40	44	128	26
PAO 460	9	110.89	40	50	140	19
PAO 680	9	111.69	41	43	127	26

Table 12: Design variables obtained without scuffing constraint for stage 3.

ISO VG	m_3	b_3	Z_1	Z_2	β_3	h_3	d_{s3}
PAO 220	6.5	071.84	096	31	8.001	2	10
PAO 460	6.5	068.38	100	33	8.000	1	10
PAO 680	9.0	090.28	101	33	8.006	1	15

Table 13: Minimum objective function values for weight and power loss without scuffing constraint

ISO VG PAO	Weight, kg	Power loss, kW
220	4064.49	18.49
460	4207.55	17.24
680	4373.26	16.57

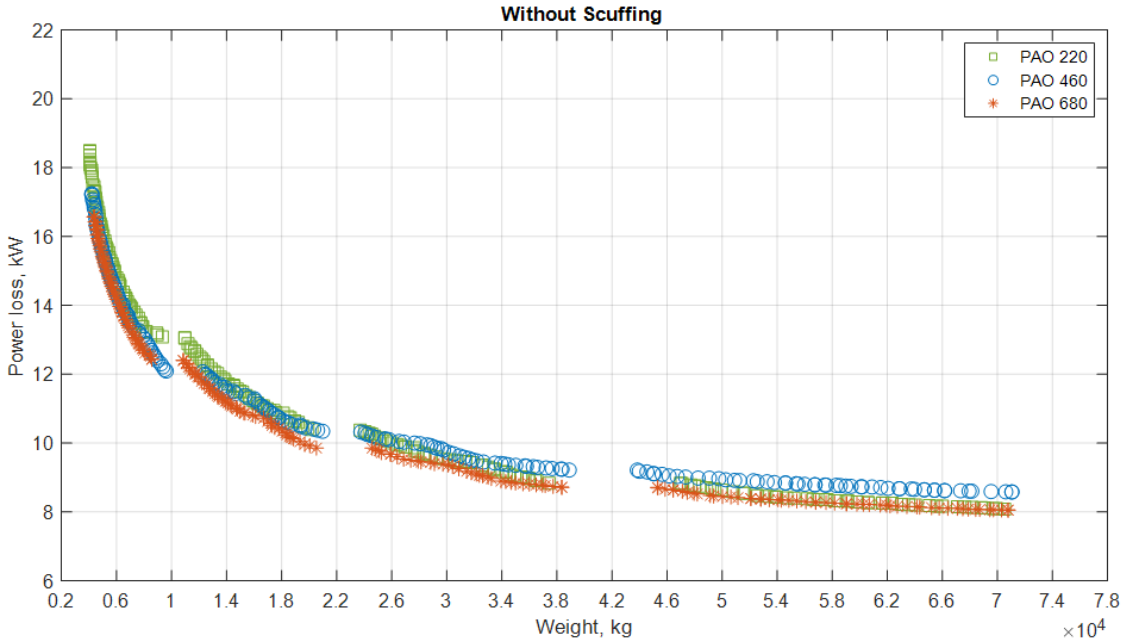

Figure 5: Pareto fronts for three different grades of oil without scuffing constraint.

CONCLUSIONS

Multi-objective optimization of WTG was carried out by considering two fitness functions: minimizing weight and minimizing power loss with all regular mechanical design constraints, critical planetary constraints, and scuffing constraints. It concluded that,

a) Single-objective optimization for spur gear pair with all constraints (including scuffing) improved efficiency by 0.605%, respectively, for unmodified, smooth meshing, and high load capacity gear tooth profile when results were validated with commercial gear software KISSsoft.
b) For advanced gearboxes such as wind turbine gearboxes, multi-objective optimization was done, and it was investigated that ISO VG PAO 680 outperforms the other grades of oils for all gear involute profiles. Hence PAO 680 was recommended to use in the wind turbine gearbox as risk of scuffing was low.
c) As risk of scuffing was low for the first two planetary arrangements, hence it is recommended to use multi-stage of planetary gear trains for higher power capacity in the wind turbine application.

Hence, it was clear from the study that a complex gearbox design could fail if scuffing constraint was not considered, resulting in significantly increased risk of scuffing. Optimization of WTG (pph model) with all regular mechanical design and scuffing constraint was the novel contribution to the current study. This approach could be extended by including helical planetary gear trains, manufacturing constraints, along with the optimization in fault diagnosis and noise reduction aspects.

APPENDIX A

Parameter	Symbol	Value	Unit
Gear material's bending strength	σ_{FP}	301	N/mm^2
Gear material's contact strength	σ_{HP}	1088	N/mm^2
Gear material's density	ρ_{mg}	7.8×10^{-6}	kg/mm^3
Shaft material's ultimate strength	S_u	827	N/mm^2
Shaft material's yield strength	S_y	455	N/mm^2
Shaft material's density	ρ_{ms}	7.8×10^{-6}	kg/mm^3
Low speed stage sun and planet surface roughness	R_a	0.5	μm
Intermediate and high-speed stage pinion-gear surface roughness	R_b	0.7	μm
Number of bearings	N_b	12	–
Rim thickness factor	K_B	1.0	–
Overload factor	K_O	1.0	–
Size factor	K_S	1.0	–
Load distribution factor	K_H	1.0	–
Bending strength's stress cycle life factor	Y_N	1.0	–
Temperature factor	Y_θ	1.0	–
Reliability factor (99%)	Y_Z	1.0	–
Pitting stress cycle factor	Z_N	1.0	–
Pitting resistance's surface factor	Z_R	1.0	–
Pitting resistance's hardness ratio factor	Z_W	1.0	–
Quality factor	Q	9	–
Poisson's ratio	μ	0.3	–
Thermal contact coefficient of gear material	B_{M1}, B_{M2}	13.6	$N/ms^{0.5}K$
Hardness of gear material	H	400	BHN
Modulus of elasticity	E	206	GPa

NOMENCLATURE

a_1	Center distance between gear pair, [mm]
a_e	Center distance between sun and planet gear, [mm]
a_i	Center distance between planet and ring gear, [mm]
b_H	Semi-width of Hertzian contact band, [mm]
b_i	Face width of gear pair i, [mm]
B_{M1}, B_{M2}	Gear material's thermal contact coefficient, [$N/ms^{0.5}K$]
$C_{\alpha e}$	Contact ratio for sun-planet gear mesh, [-]
$C_{\alpha h}$	Total contact ratio for helical pair (gear-pinion), [-]
$C_{\alpha i}$	Contact ratio for planet-ring mesh, [-]
d	Inside diameter of planet bearing or planet pin diameter, [mm]
d_i	Gear pitch circle diameter i, [mm]
d_{bg}	Gear base circle diameter, [mm]
d_{bp}	Pinion base circle diameter, [mm]

d_{og}	Gear outside circle diameter, [mm]
d_{op}	Pinion outside circle diameter, [mm]
d_p	Planet gear pitch circle diameter, [mm]
d_{pb}	Planet gear base circle diameter, [mm]
d_{po}	Planet gear outside diameter, [mm]
d_r	Ring gear pitch circle diameter, [mm]
d_{rb}	Ring gear base circle diameter, [mm]
d_{ri}	Ring gear inside diameter, [mm]
d_{ro}	Ring gear outside diameter, [mm]
d_{rp}	Planet gear root circle diameter, [mm]
d_{rs}	Sun gear root circle diameter, [mm]
d_s	Sun gear pitch circle diameter, [mm]
d_{sb}	Sun gear base circle diameter, [mm]
d_{si}	Shaft diameter i, [mm]
d_{so}	Sun gear outside diameter, [mm]
E	Modulus of elasticity, [kN/mm^2]
F	Bearing load, [N]
F_t	Transmitted tangential load, [N]
H_V	Gear power loss factor, [-]
K	Flash temperature constant
K_O	Overload factor, [-]
K_V	Dynamic factor, [-]
K_S	Size factor, [-]
K_H	Load distribution factor, [-]
K_B	Rim thickness factor, [-]
k_{sump}	Lubrication parameter type, [-]
l_p	Length of planet pin, [-]
M_{max}	Shaft's maximum bending moment, [N.mm]
m_i	Module of gear pair i, [mm]
m_n	Normal module, [mm]
m_t	Transverse module, [mm]
M_b	Mass of bearing, [kg]
n_1	Rotational speed, [rpm]
N_{CP}	Number of planet gears, [-]
N_b	Number of bearings, [-]
P	Power Capacity, [kW]
P_{VD}	Seal power loss, [W]
P_{VL}	Bearing friction power loss, [W]
P_{VZP}	Gear mesh friction power loss, [W]
$P_{scuf\ (e)}$	Probability of scuffing risk for sun-planet gear mesh, [-]
$P_{scuf\ (h)}$	Probability of scuffing risk for gear pair, [-]
$P_{scuf\ (i)}$	Probability of scuffing risk for planet-ring gear mesh, [-]
Q	Quality factor, [-]
R_a	Low speed sun and planet surface roughness, [μm]
R_b	Intermediate and high-speed gear surface roughness, [μm]

S_u	Shaft material's ultimate strength, [N/mm^2]
S_y	Shaft material's yield strength, [N/mm^2]
S_e	Shaft material's endurance limit, [N/mm^2]
T	Torque on shaft, [N.mm]
v	Peripheral speed, [m/s]
v_{r1}, v_{r2}	Pinion and gear rolling velocities, [mm/s]
u_o	Overall gear transmission ratio, [-]
u	Stage gear ratio, [-]
w_n	Normal unit load, [N/mm]
X_Γ	Load sharing factor, [-]
Y_N	Bending strength's stress cycle life factor, [-]
Y_J	Bending strength's geometry factor, [-]
Y_θ	Temperature factor, [-]
Y_Z	Reliability factor, [-]
Z_E	Elastic coefficient, [[N/mm^2]$^{0.5}$]
Z_R	Pitting resistance's surface factor, [-]
Z_I	Pitting resistance's geometry factor, [-]
Z_N	Pitting stress cycle factor, [-]
Z_W	Pitting resistance's hardness ratio factor, [-]
α	Pressure angle, [°]
α_t	Transverse pressure angle, [°]
α_{wt}	Transverse operating pressure angle, [°]
β	Helix angle, [°]
η_{oil}	Dynamic viscosity of oil at operating temperature, [mPas]
$\theta_{B\,max}$	Maximum contact temperature, [°C]
$\theta_{fl\,max}$	Maximum flash temperature, [°C]
θ_m	Tooth temperature, [°C]
θ_{oil}	Temperature of Oil, [°C]
μ	Coefficient of friction in bearing, [-]
μ_m	Average coefficient of friction, [-]
v_{40}	Kinematic viscosity at 40°C, [mm^2/s]
ρ_n	Normal relative radius of curvature, [mm]
ρ_{mg}	Gear material's density, [kg/mm^3]
ρ_{ms}	Shaft material's density, [kg/mm^3]
σ_{FP}	Gear material's bending strength, [N/mm^2]
σ_{HP}	Gear material's contact strength, [N/mm^2]

REFERENCES

AGMA 6123-C16. (2016). Design manual for enclosed epicyclic gear drives.

AGMA 925-A03. (2001). Effect of lubrication on gear surface distress.

Akay, B., Ragni, D., Ferreira, C. S. & Bussel, G. J. W. Van. (2013). Investigation of the root flow in a Horizontal Axis. Wind Energy, 1–20. https://doi.org/10.1002/we

American Gear Manufactures Association. (2004). ANSI/AGMA 2001-D04 Fundamental Rating Factors and Calculation Metrhods for Involute Spur and Helical Gear Teeth. 04, 66. ANSI/AGMA 2001-D04

Awea, A. A. (2010). Standard for Design and Specifications of Gearboxes for Wind Turbines. 1(March).

Deb, K. (2011). Multi-objective Evolutionary Optimisation for Product Design and Manufacturing. In Multi-objective Evolutionary Optimisation for Product Design and Manufacturing. https://doi.org/10.1007/978-0-85729-652-8

Dinner, H. (2011). Micropitting in wind turbine gearboxes: Calculation of the safety factor and optimization of the gear geometry. Applied Mechanics and Materials, 86, 898–903. https://doi.org/10.4028/www.scientific.net/AMM.86.898

Fernandes, C. M. C. G., Hammami, M., Martins, R. C. & Seabra, J. H. (2016). Power loss prediction: Application to a 2.5 MW wind turbine gearbox. Proceedings of the Institution of Mechanical Engineers, Part J: Journal of Engineering Tribology, 230(8), 983–995. https://doi.org/10.1177/1350650115622362

Fernandes, C. M. C. G., Marques, P. M. T., Martins, R. C. & Seabra, J. H. O. (2015). Gearbox power loss. Part II: Friction losses in gears. Tribology International, 88, 309–316. https://doi.org/10.1016/j.triboint.2014.12.004

Fotso, H. R. F., Kazé, C. V. A. & Kenmoé, G. D. (2021). Real-time rolling bearing power loss in wind turbine gearbox modeling and prediction based on calculations and artificial neural network. Tribology International, 163(March). https://doi.org/10.1016/j.triboint.2021.107171

Jelaska, D. (2012). Gears and Gear Drives. In Gears and Gear Drives. https://doi.org/10.1002/9781118392393

Kamble, D. N., Gadekar, T. D. & Agrawal, D. P. (2022). Experimental study on gearbox oil blended with composite additives. Jurnal Tribologi, 33(September 2021), 1–19.

Kumar, A., Ramkumar, P. & Shankar, K. (2023). Multi-objective 3-stage wind turbine gearbox (WTG) with tribological constraint. Mechanics Based Design of Structures and Machines, 0(0), 1–27. https://doi.org/10.1080/15397734.2023.2249987

Li, Y. F., Xu, Y. X. & Li, G. X. (2012). Optimization design of the wind turbine gearbox based on genetic algorithm method. Materials Science Forum, 697–698, 697–700. https://doi.org/10.4028/www.scientific.net/MSF.697-698.697

Liu, G., Liu, H., Zhu, C., Mao, T. & Hu, G. (2021). Design optimization of a wind turbine gear transmission based on fatigue reliability sensitivity. Frontiers of Mechanical Engineering, 16(1), 61–79. https://doi.org/10.1007/s11465-020-0611-5

Miler, D., Lončar, A., Žeželj, D. & Domitran, Z. (2017). Influence of profile shift on the spur gear pair optimization. Mechanism and Machine Theory, 117, 189–197. https://doi.org/10.1016/j.mechmachtheory.2017.07.001

Parmar, A., Ramkumar, P. & Shankar, K. (2020). Macro geometry multi-objective optimization of planetary gearbox considering scuffing constraint. In Mechanism and Machine Theory (Vol. 154). Elsevier Ltd. https://doi.org/10.1016/j.mechmachtheory.2020.104045

Patil, M., Ramkumar, P. & Shankar, K. (2019). Multi-objective optimization of the two-stage helical gearbox with tribological constraints. Mechanism and Machine Theory, 138, 38–57. https://doi.org/10.1016/j.mechmachtheory.2019.03.037

SKF, G. (2018). Rolling bearings SKF mobile apps. Pub Bu/P1 17000/1 En ·, 88. skf.com/go/17000

Tavner, P. (2011). SUPERGEN Wind 2011 General Assembly. SUPERGEN Wind 2011 General Assembly, March.

Tian, J. M. & Tan, X. (2014). The optimization design of wind turbine gearbox based on improved genetic algorithm and feasibility analysis. Advanced Materials Research, 889–890, 107–112. https://doi.org/10.4028/www.scientific.net/AMR.889-890.107

Ukonsaari, J. & Bennstedt, N. (2016). Wind turbine gearboxes maintenance effect on present and future gearboxes for wind turbines. Energiforsk.

Ziat, A., Zaghar, H., Ait Taleb, A. & Sallaou, M. (2022). Multi-objective Optimization under Uncertainty of a Continuously Variable Transmission for a 1.5 MW Wind Turbine. SAE International Journal of Materials and Manufacturing, 15(4). https://doi.org/10.4271/05-15-04-0026